

Elicitation of potent SARS-CoV-2 neutralizing antibody responses through immunization with a versatile adenovirus-inspired multimerization platform

Christopher Chevillard,^{1,5} Axelle Amen,^{1,3,5} Solène Besson,^{1,5} Dalil Hannani,² Isabelle Bally,¹ Valentin Dettling,¹ Evelyne Gout,¹ Christophe J. Moreau,¹ Marlyse Buisson,¹ Salomé Gallet,¹ Daphna Fenel,¹ Emilie Vassal-Stermann,¹ Guy Schoehn,¹ Pascal Poignard,^{1,3,4} Marie-Claire Dagher,¹ and Pascal Fender¹

¹CNRS, Univ. Grenoble Alpes, CEA, UMR5075, Institut de Biologie Structurale, 38042 Grenoble, France; ²University Grenoble Alpes, CNRS, UMR 5525, VetAgro Sup, Grenoble INP, TIMC, 38000 Grenoble, France; ³CHU Grenoble Alpes, 38000 Grenoble, France; ⁴Department of Immunology and Microbiology, The Scripps Research Institute, La Jolla, CA 92037, USA

Virus-like particles (VLPs) are highly suited platforms for protein-based vaccines. In the present work, we adapted a previously designed non-infectious adenovirus-inspired 60-mer dodecahedral VLP (ADDomer) to display a multimeric array of large antigens through a SpyTag/SpyCatcher system. To validate the platform as a potential COVID-19 vaccine approach, we decorated the newly designed VLP with the glycosylated receptor binding domain (RBD) of SARS-CoV-2. Cryoelectron microscopy structure revealed that up to 60 copies of this antigenic domain could be bound on a single ADDomer particle, with the symmetrical arrangements of a dodecahedron. Mouse immunization with the RBD decorated VLPs already showed a significant specific humoral response following prime vaccination, greatly reinforced by a single boost. Neutralization assays with SARS-CoV-2 spike pseudo-typed virus demonstrated the elicitation of strong neutralization titers, superior to those of COVID-19 convalescent patients. Notably, the presence of pre-existing immunity against the adenoviral-derived particles did not hamper the immune response against the antigen displayed on its surface. This plug and play vaccine platform represents a promising new highly versatile tool to combat emergent pathogens.

INTRODUCTION

Although genomic vaccines have recently demonstrated their capacity to elicit protective immune responses,¹ protein-based vaccines remain highly attractive due to their lower cost, and ease of transport and storage, crucial to reach developing countries and remote locations, as well as better social acceptance, as recently highlighted by hesitancy regarding COVID-19 RNA vaccines. Protein immunogenicity is highly increased through presentation to the immune system in a multimeric manner, and a number of vaccine platforms have been developed to this aim, with various advantages and limitations.² We have previously reported that a non-infectious virus-like particle (VLP) derived from human adenovirus of type 3 and consisting of 60 identical penton base

monomers could be exploited to display epitopes of interest on its surface.^{3–5} In this vaccine platform, named ADDomer, exposed loops of the penton base protein were engineered to allow insertion of foreign peptides such as a linear neutralizing epitope from Chikungunya virus. However, this design did not permit the insertion of structurally complex antigens. To overcome this limitation while keeping the immunogenicity advantage of ADDomer, we describe here a redesigned platform offering a highly versatile capacity to display large and structurally complex antigens with potential post-translational modifications. In order to decorate the adenovirus-based VLPs with large antigens, the SpyTag/SpyCatcher system^{6–9} was combined with the ADDomer technology. In this system, derived from *Streptococcus pyogenes*, an aspartate residue from the 13 amino acid SpyTag peptide (ST) can spontaneously create a covalent bond with a lysine residue encompassed in the complementary SpyCatcher module (SC). We thus genetically inserted the sequence coding for the ST peptide into the “variable loop” of the ADDomer that was previously used for small antigen insertion, yielding a VLP with 60 potential attachment sites for complex antigens engineered with an SC anchor.

In order to assess the newly developed platform, we decided to first test it as a potential candidate vaccine to elicit neutralizing antibodies (NAbs) against the severe acute respiratory syndrome coronavirus 2 (SARS-CoV-2). SARS-CoV-2 is an enveloped positive strand RNA virus belonging to the beta-coronavirus genus from the Coronaviridae family. It is the etiological agent of coronavirus disease 2019

Received 28 October 2021; accepted 7 February 2022;
<https://doi.org/10.1016/j.ymthe.2022.02.011>.

⁵These authors contributed equally

Correspondence: Pascal Fender, CNRS, Univ. Grenoble Alpes, CEA, UMR5075, Institut de Biologie Structurale, 38042 Grenoble, France

E-mail: pascal.fender@ibs.fr

Correspondence: Pascal Poignard, CNRS, Univ. Grenoble Alpes, CEA, UMR5075, Institut de Biologie Structurale, 38042 Grenoble, France

E-mail: pascal.poignard@ibs.fr



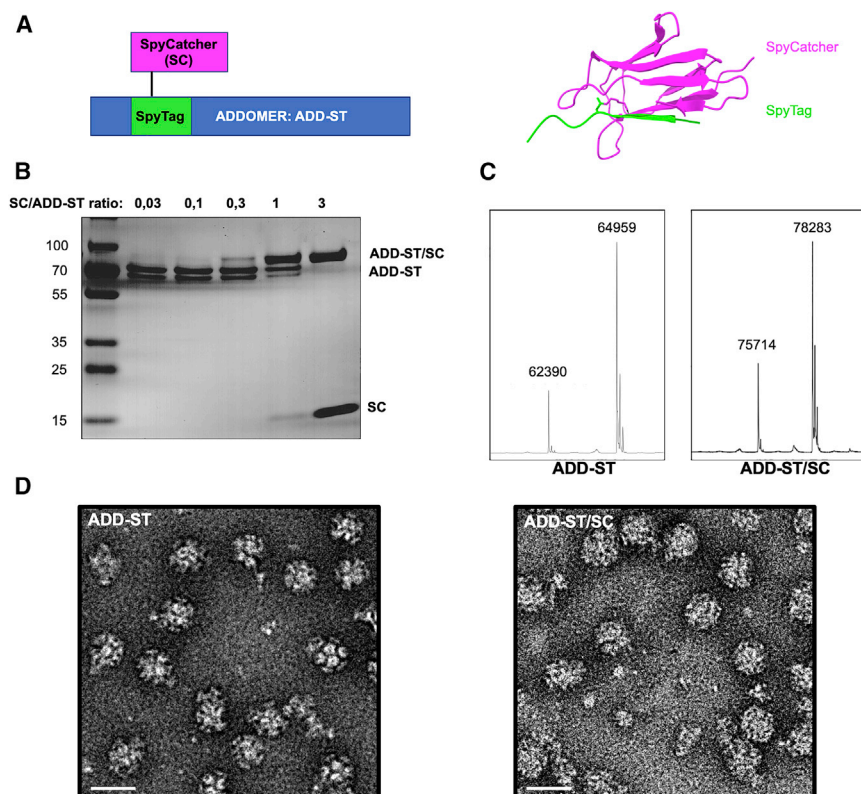


Figure 1. Application of the SpyTag/SpyCatcher cross-linking method to the ADDomer technology

(A) Diagram showing the internal insertion of SpyTag in the internal loop of an ADDomer monomer. Spytag (in green) can make an isopeptidic bond with SpyCatcher (in purple). Structure of a SpyTag covalently linked to a SpyCatcher is shown on the right (PDB code: 4MLI). (B) SDS-PAGE profile of reduced and boiled samples of ADD-ST after interaction with incremental ratio of SC showing the apparition of a higher MW covalent adduct (ADD-ST/SC). (C) Electrospray ionization graphs of ADD-ST and ADD-ST/SC showing the shift of the peaks by 13.3 kDa. The doublet is due to an alternative start of translation in ADD-ST and display the same mass shift of 13.3 kDa. (D) Negative staining electron micrographs of ADD-ST and ADD-ST/SC (bar, 30 nm).

can successfully be decorated with SARS-CoV-2 RBD and is highly immunogenic in mice, eliciting high neutralizing Ab titers.

RESULTS

Internal insertion of ST in ADDomer results in efficient SC cross-linking

ADDomer is a non-infectious 30-nm nanoparticle, formed from 12 bricks of the homo-pentameric penton base from the human adenovirus type 3. The ST sequence was inserted in the

ADDomer gene in a region coding for the exposed flexible loop called the variable loop (Figure 1A). Due to the spontaneous homo-oligomerization of the 12-pentameric penton base, 60 copies of ST are exposed on the surface of the ADDomer-ST (ADD-ST) particle. To assess whether the newly inserted ST sequence was accessible and functional on ADD-ST, incubation with a different ratio of SC was performed. After boiling of samples, SDS-PAGE profile clearly showed that the incremental SC/ADD-ST ratio is correlated with the apparition of a band of higher molecular weight and the decrease of the intensity of bands related to unlinked moieties. Importantly, there was no remaining signal for undecorated ADD-ST after SC addition at the highest ratio, thus reflecting the full decoration of the nanoparticle (Figure 1B). This result suggests an efficient and concentration-dependent formation of the ADD-ST/SC complex. Mass spectrometry analysis confirmed that the ADD-ST doublet shifted by 13.3 kDa (Figure 1C), which corresponds to the molecular weight (MW) of SC. The two peaks observed in mass spectrometry is due to a second initiation codon in ADD-ST (starting at Methionine 25) without affecting the particle stability,²⁸ and SC can bind to each form indifferently, as shown by a similar shift of their MW corresponding to the addition of SC. Negative staining electron microscopy imaging performed on ADD-ST alone and ADD-ST fully decorated by SC showed that the integrity of the particle was not affected by the presence of SC and the grainy appearance of ADD-ST/SC likely reflects the presence of SC at the particle surface (Figure 1D). Altogether, these data show that SC cross-linking to ADD-ST is operational and can result in saturated decoration of the nanoparticle.

(COVID-19), and at the origin of the pandemic that started in December 2019, leading to 5,542,359 deaths as of January 19, 2022 (<https://covid19.who.int/>), and vast socio-economic consequences.¹⁰ Protection against SARS-CoV-2 infection and COVID-19 can be mediated by neutralizing Abs targeting the envelope trimeric glycoprotein spike (S) exposed at the surface of the virus.^{11,12} Accordingly, spike-based vaccine approaches eliciting SARS-CoV-2 NAb responses have been successful at preventing COVID-19.^{13–15} The ectodomain of the S protein is divided into the S1 and S2 domains. The Spike protein binds to the host angiotensin-converting enzyme 2 (ACE2), which serves as an entry receptor, as previously reported with SARS-CoV, responsible for the 2002–2004 SARS outbreak.^{16–19} A subdomain of S1, named receptor binding domain (RBD), is the contact interface between the virus and the ACE2 receptor. Numerous studies have shown that the RBD comprises multiple distinct antigenic sites and is a prime target for NABs in COVID-19 convalescent patients.^{20–23} These NABs²⁴ strongly inhibit cell infection by SARS-CoV-2 by competing with the RBD-ACE2 interaction. Moreover, anti-RBD NABs have been shown to confer protection against SARS-CoV-2 challenge in animal models of COVID-19, as well as to prevent COVID-19 in humans, thus confirming the interest of using RBD as a vaccine immunogen.^{25–27}

This prompted us to use the RBD as the antigen to be displayed on our newly designed VLP platform in order to engineer a novel COVID-19 vaccine approach. Here, we report that the newly designed platform

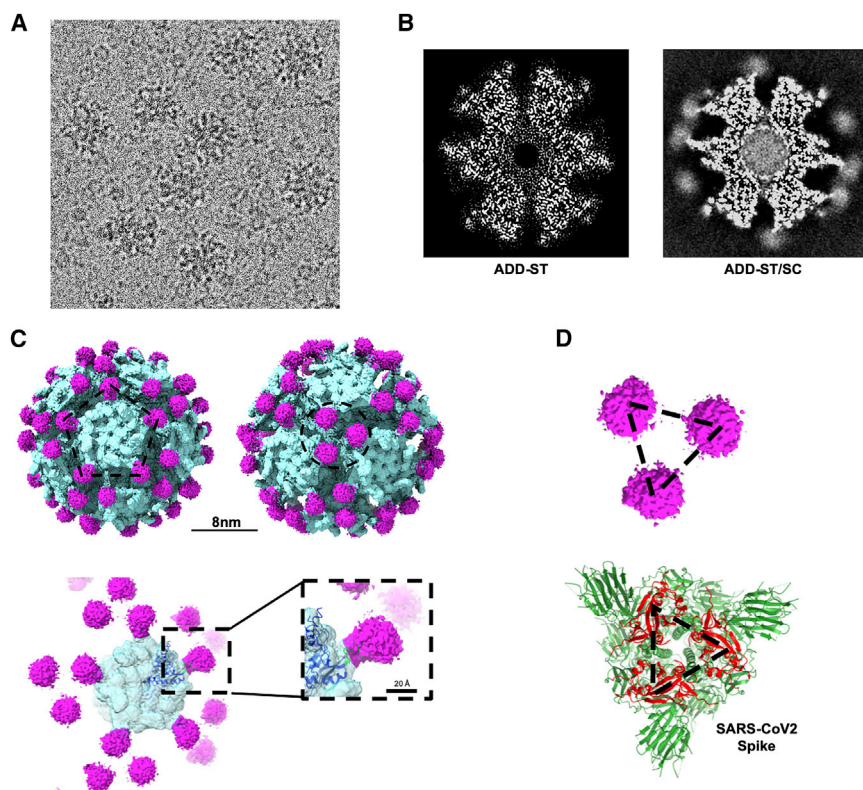


Figure 2. Cryo-EM reconstruction of ADD-ST decorated with SC

(A) Representative 2D picture of the particles frozen on ice (bar, 30 nm). (B) Section through the density of the 3D reconstruction without (ADD-ST) or with SC (ADD-ST/SC). (C) Isosurface representation of the ADDomer-ST/SC 3D structure showing the extra density of SC in purple onto the non-decorated ADD-ST scaffold in light blue. The particle is represented along either the 5- or 3-fold-axis (left and right, upper panel; bars, 80 and 20Å, respectively). Focus on a pentameric complex of ADD-ST/SC with a close-up view onto a single SC/ST interaction (dashed line boxes in the lower panel). The atomic resolution structure (dark blue) of the HAd3 penton base (PDB 4AQQ) has been fitted into the ADDomer EM density (light blue). (D) Organization of SC along the 3-fold axis of the particle (upper panel) and comparison with SARS-CoV-2 RBD architecture (in red) within the Spike protein structure (in green, PDB 6VXX) at the same scale.

Cryoelectron microscopy analysis enables visualization of SC decoration on ADD-ST

In order to visualize the SC arrangement around the ADDomer particle, a structural study by cryoelectron microscopy (cryo-EM) was used. Fully decorated ADD-ST/SC particles were imaged on a Glacios electron microscope (Figure 2A). Image analysis was performed and the obtained 3D structure was compared with the structure of an undecorated ADDomer particle (EMD-0198). An extra-density corresponding to SC bound to the ADDomer “variable loop” was clearly visible in ADD-ST/SC both in the density slice of the 3D map (Figure 2B) and in the isosurface representation of the structure (Figure 2C, purple density and supplementary movie). The resolution of the ADDomer particle is around 2.8 Å, allowing to clearly see the aminopeptidic chain. However, the ST/SC part is not rigidly attached to the ADDomer, which explains why the corresponding density is fuzzy, and the structure not better defined (Figure S1). The ADDomers have 2, 3, and 5 axes of symmetry (the latter two are shown in Figure 2C), which is a characteristic of a dodecahedron, meaning that SCs are distributed accordingly. Interestingly, along the 3-fold axis, SCs are ~4.7 nm apart, which is close to the RBD in the trimeric spike protein of SARS-CoV-2 (~4.1 nm), suggesting that the decorated particles would closely mimic the natural trimeric arrangement of RBDs (Figure 2D). Both the multivalency of SC displayed by the particle and the arrangements they have around the different symmetry axis could be an asset for vaccination purpose if an antigen is fused to this module.

Secreted RBD fused to SC is glycosylated and can be displayed at different ratios on the ADD-ST particle

To take advantage of the spontaneous and covalent linking of SC to ADD-ST, we reasoned that SC could be used as a versatile carrier to easily and efficiently fuse antigens, like in this SARS-CoV-2 vaccine development (Figure 3A), and in broader perspectives to diverse soluble proteins

of interest. In the present study, the SARS-CoV-2 RBD was fused to the N-terminus of the SC (RBD-SC) and a melittin signal peptide was added to allow protein post-translational modifications (PTMs) such as glycosylations and secretion from insect cells. To assess whether the secreted and purified RBD-SC was glycosylated, it was treated with N-glycosylase (PNGaseF), and the result showed a shift in the migration of the related band in SDS-PAGE gel, indicating that RBD-SC was indeed glycosylated (Figure 3B). As previously performed with unfused SC (Figure 1B), incremental amounts of RBD-SC were added to ADD-ST in order to decorate the particle with different ratio of cargos (from 0.03 to 3 copies of SC *per* particle monomers). The SDS-PAGE gel profile (Figure 3C) showed the correlated apparition of a band at higher MW with increased concentrations of RBD-SC. This result reflects the covalent linking of RBD-SC to the ADD-ST monomers, whereas the band corresponding to non-decorated ADD-ST monomer progressively faded away, disappearing when the particle is fully decorated. This result showed that the ADDomer platform can be decorated with different numbers of antigen copies exposed on its surface. Altogether, these experiments demonstrated that SC fusion to large antigens (~40 kDa for RBD-SC) with post-translational modifications enable their covalent linking to the ADDomer platform and that the ratio of decoration can be adjusted according to desired applications.

ADDomers decorated of glycosylated RBD bind to ACE2

RBD is the subdomain of the SARS-CoV-2 spike protein that binds to the human ACE2 receptor. To assess the function of RBDs

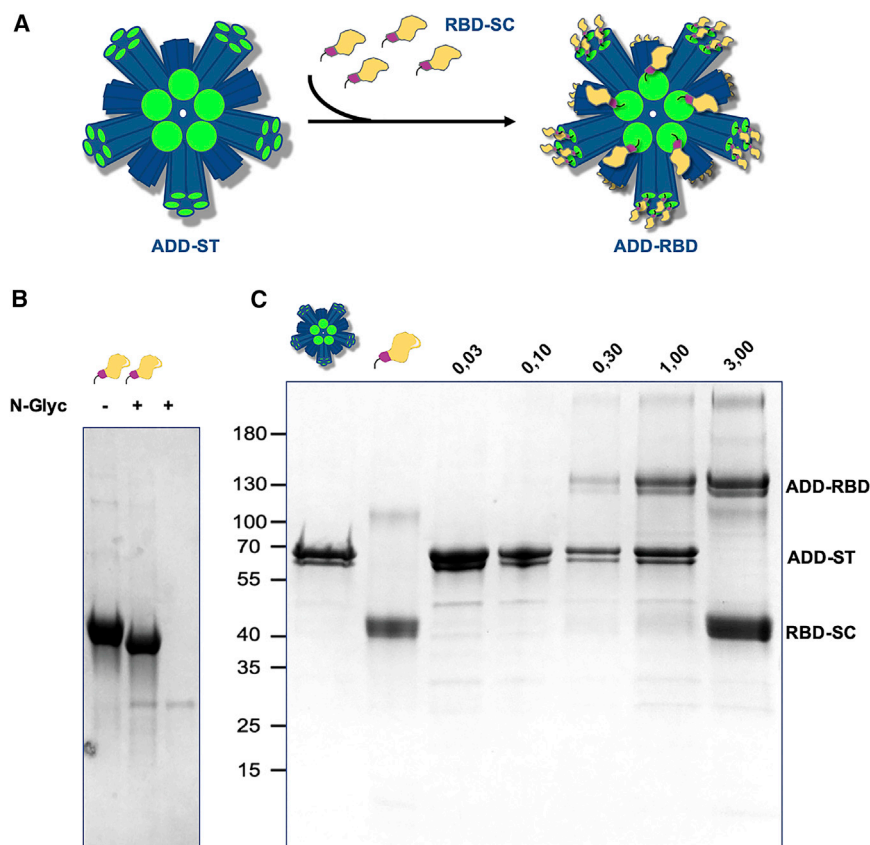


Figure 3. Fusion of SARS-CoV-2 RBD to SC enables its surface presentation on ADDomer particles

(A) Schematic representation of the spontaneous RBD-SC binding to ADD-ST to give ADD-RBD. (B) SDS-PAGE gel with RBD-SC before (–) and after (+) treatment with N-glycosidase and in absence of SC-RBD. The decrease of the molecular weight of SC-RBD after treatment indicates that it is glycosylated. (C) SDS-PAGE gel of reduced and boiled samples showing from left to right, the marker, bands of ADD-ST alone, SC-RBD alone and a fix amount of ADD-ST incubated with different ratio of RBD-SC (*per particle monomer*). The additional upper bands reflect the covalent adduct between ADD-ST and RBD-SC and thus the apparition of ADD-RBD. As expected, the increasing intensities of the ADD-RBD bands correlate with a decrease of non-decorated ADD-ST monomer.

linked to the ADDomer particles, three different approaches were used. First, binding experiments at the molecular scale were performed using surface plasmon resonance (SPR) on immobilized dimeric human ACE2 fused to the Fc domain of human immunoglobulin (Ig)G.²⁹ Sensorgrams of ADD-RBD binding to immobilized human ACE2 showed a clear concentration-dependent binding of the RBD-decorated particles on ACE2 and a stable interaction with no visible dissociation at the end of injections (Figure 4A). The extremely slow dissociation rate ($4.57 \times 10^{-4} \text{ s}^{-1}$) agreed with a sub-nanomolar “apparent” K_D ($3.09 \times 10^{-10} \text{ M}$). This apparent K_D is the result of an avidity with the decorated particle effect since the K_D of RBD-SC alone is slightly higher ($1.53 \times 10^{-8} \text{ M}$; Figure S2). In any case, this result showed that the RBD is functional and that our platform somehow mimics viruses that evolved to take advantage of multivalent interactions with cellular receptors. In a second experiment at the cell scale, the direct binding of ADD-RBD onto HeLa cells stably expressing ACE2 was visualized by immunofluorescence using anti-ADDomer antibodies. The green signal seen at the periphery of HeLa-ACE2 cells in the presence of ADD-RBD contrasted with the absence of signal observed with the same cells but in presence of undecorated ADD-ST particles. This result demonstrated that RBD at the surface of the particles induced the interaction with ACE2 present at the surface of the HeLa-Ace2 cells (Figure 4B). Finally, a competition experiment between a

pseudo-typed virus harboring the SARS-CoV-2 spike and either RBD-SC or ADD-RBD was performed. Negative control was made with undecorated ADD-ST alone. As expected, both RBD-SC alone and ADD-RBD were able to compete with the pseudo-typed virus with a slightly higher efficiency for the RBD-decorated particle (Figure 4C). Altogether, these experiments showed that RBD-SC is properly folded and can bind the ACE2 receptor at the molecular and cellular

RBD-decorated ADDomer elicits rapid anti-CoV2 Ab responses in mice, not negatively impacted by adenovirus pre-immunity

Multivalent exposition of RBD antigens at the surface of the particle is likely to result in a better activation of the humoral system than RBD alone. However, one cannot exclude that ADDomer itself could also play an indirect role in the anti-SARS-CoV-2 response, especially in a population with pre-existing adenovirus immunity. To address these two points, four groups of 10 mice were designed (Figure 5A). The two first control groups were injected with RBD-SC alone in group 1 or with the same amount of unlinked RBD-SC plus naked-ADDomer (i.e., not displaying the antigen) in group 2. The two other groups (groups 3 and 4) were vaccinated with ADD-RBD (i.e., RBD displayed at the particle surface) but group 4 was pre-immunized with naked-ADDomer 2 weeks before the injection of ADD-RBD, in order to investigate whether anti-HAdV-3 penton base antibodies, as may possibly be found in individuals previously infected with adenovirus type 3, may impact the immunogenicity of ADD-RBD (Figure 5B). The presence of anti-ADDomer (i.e., HAdV-3 penton base adenovirus) antibodies in group 4 was checked by ELISA 1 day before the first immunization with ADD-RBD. The results (Figure S3) show that all group 4 mice did mount an antibody response against naked-ADDomer. Then, the immune response against RBD

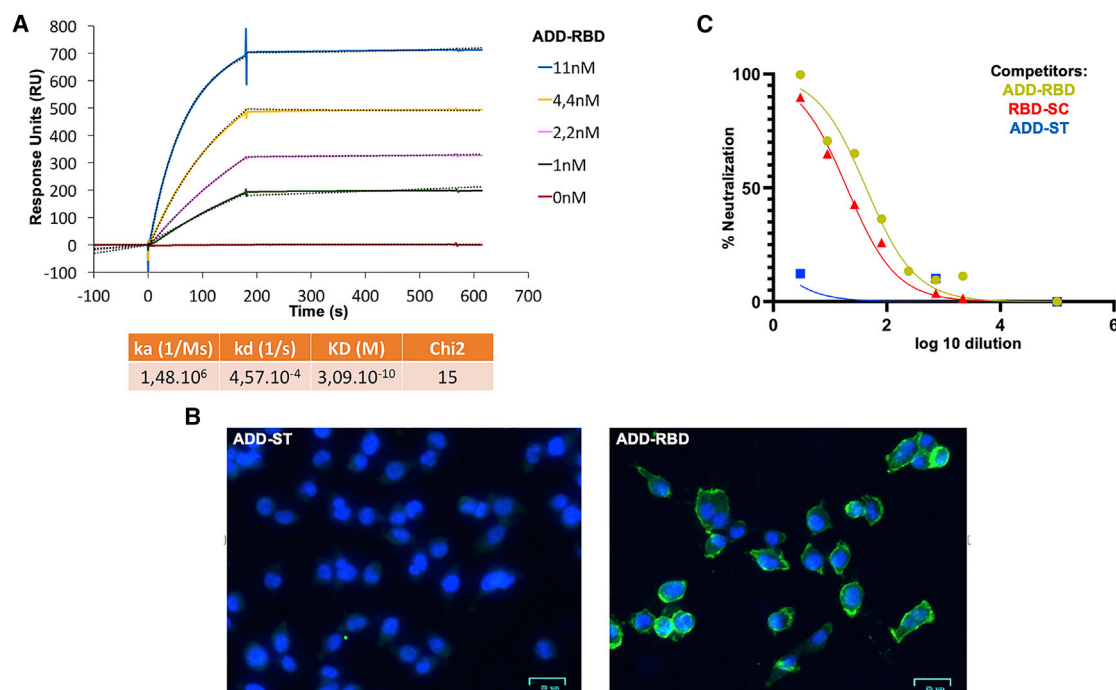


Figure 4. Functional characterization of the ADDomer particles decorated with SARS-CoV-2 RBD

(A) Surface plasmon resonance sensorgrams obtained by injection of different amounts of ADD-RBD to the immobilized ectodomain of the human ACE2 receptor fused to IgG Fc constant domain²⁹ and kinetic analysis. (B) Immunofluorescence microscopy images of HeLa-ACE2 cell at 4°C with double staining with Hoechst (blue) and anti-ADDomer Ab and an Alexa 488-conjugated secondary Ab (green) in presence of non-decorated ADD-ST (left) or ADD-RBD (right) particles. (C) Competition of pseudotyped SARS-CoV-2 virus encoding luciferase with either ADD-ST (blue), RBD-SC (red) and ADD-RBD (gold) at different dilutions.

was monitored by ELISA at days 13 (post first immunization), 27, and 41 (post second immunization). The RBD-decorated particles induced a significant anti-SARS-CoV-2 response after the first immunization (day 13, Figure 5C), whereas no response was detectable in controls of group 1 (RBD-SC alone) or group 2 (ADDomer with not displayed SC-RBD). Interestingly, anti HAdV-3 penton base pre-immunity did not negatively impact the anti-RBD response. A trend toward a stronger anti-RBD response was even observed at this stage.

Immunization boost increases both the amplitude and the duration of the response induced by ADD-RBD particles, independently of the anti-vector immunity

Two weeks after the second immunization (day 27), the anti-RBD response was clearly boosted for groups 3 and 4 that were injected with ADD-RBD, whereas the control groups 1 and 2 showed more heterogeneous responses (Figure 6A). This observation confirms that our vaccine platform displaying multivalent RBD antigens yields a rapid and efficient humoral response. The ADDomer technology applied to RBD antigen also demonstrated a long-lasting immunogenic effect with anti-SARS-CoV-2 RBD antibodies remaining at the highest level at day 41 (Figure 6B). The difference between mice pre-immunized by ADDomer (group 4) or not (group 3) was less pronounced than after the first immunization, both groups reaching high and comparable levels. Altogether, these results showed that the sec-

ond immunization enabled a high and long-lasting Ab response against the SARS-CoV-2 RBD using the ADDomer platform and that anti-vector pre-immunity is possibly beneficial in particular to the initial responses (Figure 6C).

RBD-decorated ADDomer immunization elicits strong neutralizing Ab responses

Since the RBD is critical for binding to the SARS-CoV-2 receptor ACE2, antibodies elicited through immunization with the RBD (RBD-SC or ADDomer-RBD) can hinder the interaction between the Spike proteins and ACE2, blocking viral entry. The ability to neutralize the virus depends on the affinity of the antibodies for the RBD domain, as well as on the epitope recognized. To assess the potency and efficacy of the antibodies induced in the four immunized groups of mice, the neutralization potency of sera (day 41) from vaccinated mice was assessed using SARS-CoV-2 spike (Wuhan strain) pseudo-typed lentivirus and ACE2-expressing HeLa cells. Only a partial and heterogeneous neutralization was obtained from group 1 and 2 sera in which RBD-SC was not displayed on ADDomer, even after two immunizations (Figure 7A, upper panels). Of note, sera from mice immunized with RBD-decorated ADDomer (groups 3 and 4) showed a better neutralization titer after a single immunization than groups 1 and 2 after 2 immunizations (Figure S4). After the second immunization, strong virus neutralization was observed in all mice from groups 3 and 4

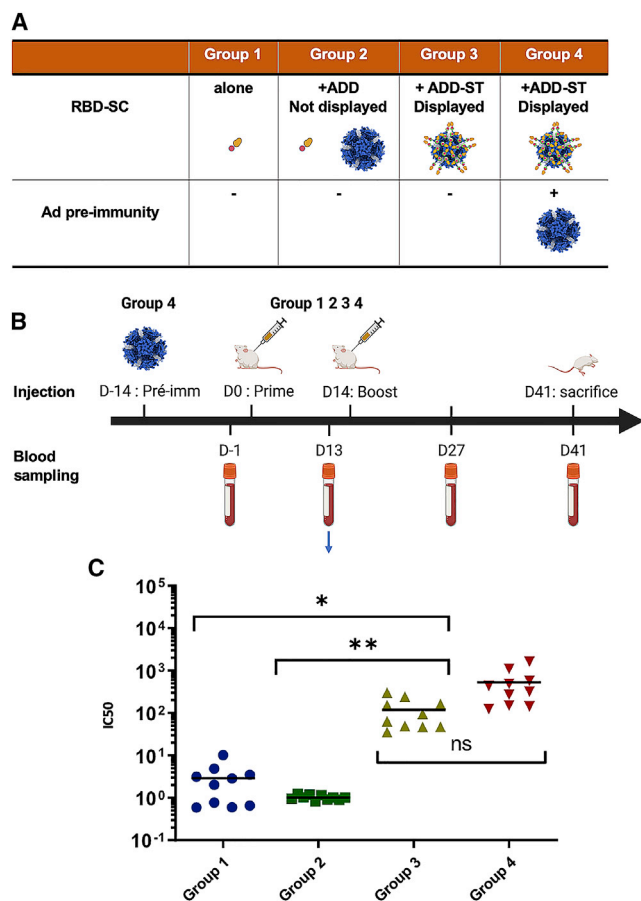


Figure 5. Immunization studies on mice inoculated with the same amount of RBD under different conditions

(A) Different groups were constituted to address the respective role of RBD-SC alone (group 1), RBD-SC in presence of naked-ADDomer (group 2), and RBD-SC displayed by ADDomer (ADD-RBD) either in adenovirus naïve or adenovirus pre-immunized mice (group 3 and 4 respectively). (B) Immunization schedule and blood sampling for all groups. (C) IC₅₀ of anti RBD response 13 days after the first immunization (n = 10). Lines are mean values and Kruskal-Wallis tests, were performed followed by a Dunn's multiple comparison tests.

(Figure 7A, lower panels). Neutralization titers (ND₅₀) clearly showed that mice vaccinated with RBD-decorated ADDomer had significantly higher neutralizing activity than mice immunized with the same amount of antigen when not displayed on the platform (Figure 7B). Moreover, in accordance with the ELISA results (Figure 5C), the anti-vector response (group 4) slightly increased the neutralization titer compared with the naïve group (group 3), which emphasizes that a pre-existing HAdV-3 penton base immunity could be beneficial for our novel vaccine platform (Figure 7B). The neutralizing Ab titers reached in groups 3 and 4 were overall superior to those from a cohort of convalescent COVID-19 patients composed of 50% mild (oxygen below 2 L/min) and 50% severe (intensive care unit) cases, and measured at 6 months after hospitalization (Figure 7B).³⁰

DISCUSSION

In this study, we designed a novel and highly versatile vaccine platform amenable to large antigens by adapting the ST/SC technology to ADDomer, an adenovirus-inspired VLP.^{5,6} This technology has already been described for designing VLP-derived vaccine; however, in these approaches, SC was the moiety grafted to the VLPs while the antigens were fused to the ST.^{7,31} In our novel vaccine technology, we used the opposite configuration with ST insertion in an internal loop of ADDomer, which minimized the risk of steric hindrance and functional impact on the spontaneous oligomerization of ADDomers. Insertion of ST in a surface-exposed loop of ADDomer did not impair the spontaneous assembly of 12 pentameric bricks (Figure 1D), thus creating a universal generic platform for multivalent antigen display. Experiments of saturating cross-linking with SC alone suggested that a full decoration (i.e., 60 copies) of the particle can be achieved (Figure 1B). Despite the flexibility of the loop in which ST was inserted, cryo-EM reconstruction of the ADD-ST/SC complex clearly showed an extra density corresponding to the SC interacting with ST fused to the ADDomer. The data thus strongly suggested that the ADDomer could be used to display a multimerized array of antigens, a property that is crucial for the elicitation of strong Ab responses.^{32–34} Interestingly, the characteristic 2-, 3-, and 5-fold symmetry axis of a dodecahedron are easily visible in the 3D structure (Figure 2C), this spatial configuration showing that the SCs are distributed at different distances from each other according to the symmetry axis. Such distribution of the antigen could potentially further favor the immunogenicity of the VLP by offering different patterns of presentation of the antigen at the particle surface.

The COVID pandemic led us to first evaluate our newly designed platform as an anti-SARS-CoV-2 vaccine to be displayed through fusion to the SC N-terminus. It is worth noting that in the 3-fold axis of ADDomer, the SC adopts a pseudo-trimeric arrangement, which on the RBD decorated VLP closely mimics the tridimensional configuration of this domain in the SARS-CoV-2 spike glycoprotein (Figure 2D). The distance between SC in such configuration is 4.7 nm, which is in the same range as that between RBDs in the trimeric Spike protein (4.1 nm). Expressing soluble RBD fused to SC in insect cells resulted in N-glycosylation as expected,³⁵ and did not affect the structure of SC, which retained its ability to cross-link to the ADD-ST vaccine platform in a dose-dependent manner (Figure 3C). The proper folding of the glycosylated RBD exposed at the surface of the particles and its ability to bind ACE2 were assessed in a functional viral entry assay via competition with SARS-CoV-2 Spike pseudo-typed virions (Figure 4C). An SPR experiment confirmed the high-affinity interaction of ADD-RBD to ACE2, the highly stable interaction observed suggesting an avidity effect of the multivalent particle exposing multiple copies of RBD (Figure 4A). Moreover, this experiment also shows that expressing RBD in insect cells leads to a functional SARS-CoV-2 glycoprotein domain. Several vaccines using the baculovirus expression system in insect cells have been approved, such as vaccines against papillomavirus or hepatitis B. The Novavax COVID-19 vaccine candidate, based on an insect cell-produced trimeric S protein, is also advancing toward approval trials.³⁶

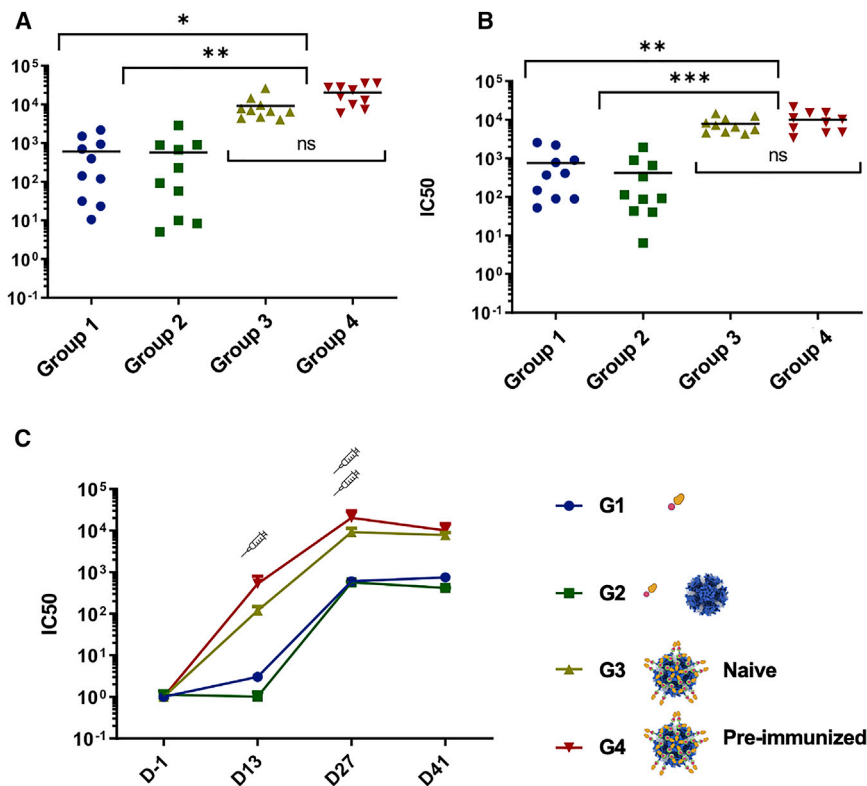


Figure 6. Anti-RBD Ab in all groups of mice 2 and 4 weeks after the booster immunization

(A) IC50 of anti-RBD for each individual mice from all groups, 2 weeks after the booster injection. (B) Same data, 4 weeks after the booster injection. Lines are mean values. Kruskal-Wallis tests, were performed followed by a Dunn's multiple comparison tests. (C) Means of the anti-RBD response from all mice according to their groups and the time after the first immunization performed at day 0.

The ability of the RBD-decorated ADDomer to elicit an anti-SARS-CoV-2 humoral response was then studied in mice. As expected, we confirmed that displaying the RBD in a multimerized manner led to a strong improvement in immunogenicity (groups 3 and 4 versus groups 1 and 2). Indeed, this was clearly apparent from the first injection, where the groups with decorated particles showed a significant anti-RBD response at day 13 as measured in ELISA (Figure 5C), whereas no response was observed for the other groups. This observation is in agreement with experiments reported with other vaccine platforms that showed that injection of RBD or S-trimer alone did not produce significant responses.^{31,37} In our experiment, we chose to inject 5 μ g of RBD, but a dose-response study would be necessary to determine the optimal amount. As a comparison, similar experiments carried out with a similar 60-mer platform showed that 0.9 μ g instead of 5 μ g of RBD resulted in a similar immune response paving the way to dose-sparing.³⁸ After the second immunization, although a response was observed in the non-decorated groups, the titers attained in the decorated groups were about 10-fold greater (Figure 6A). Notably, the anti-RBD response in the latter groups endured over time with similar titers at 2 and 4 weeks following the second immunization (Figure 6B). The anti-SARS-CoV-2 RBD sera were further assessed for their capacity to neutralize S-protein pseudotyped lentivirus particles (Figure 7). As seen for binding responses, a neutralizing activity was observed in the RBD-decorated groups after the first immunization. Overall, a good correlation between ELISA and neutralizing titers was observed. Strong neutralizing titers were attained in all mice immunized with ADD-RBD after the boost immu-

nization, superior to those of convalescent COVID-19 patients (Figure 7B), showing the ability of our vaccine platform to elicit functional Ab responses with a potential protective activity. The low titers obtained in mice immunized with RBD and naked ADDomer (no decoration) again demonstrated that the high immunogenicity achieved with decorated VLPs originated from the multimeric display of the antigen. A limitation of our study is that cellular responses were not measured. It is known that CD8 T cell responses likely play an important role in protecting against severe forms of COVID-19. In contrast to mRNA and viral vector vaccines, VLPs are not optimal platforms to elicit CD8 T cell responses, due to the lack of endogenous antigen production. This hurdle may indeed represent a limitation for such vaccines, including our approach. However, CD8 responses may be elicited by VLPs under certain circumstances through cross-presentation following uptake by dendritic cells, and additional work will be necessary to evaluate whether ADDomer may potentially elicit specific CD8 T cells.

Overall, the data are in adequacy with results obtained with similar vaccine platforms using multimeric display of the SARS-CoV-2 RBD on scaffolds such as the 24-mer ferritin, the 60-mer dodecahedral thermophilic aldolase.^{31,39,40,41} In contrast to these latter vaccine platforms, our particles originate from a human virus, Adenovirus serotype 3 (HAd3), which is known to have a relatively high seroprevalence.^{42,43}

However, if HAdV-3 is globally among the most common types implicated in HAdV infections, a great variation is observed by geographic regions. Indeed, HAdV-3 accounts for 15% to 87% of adenoviral respiratory infections with a greater prevalence in Asia than in western countries.⁴⁴ Neutralizing antibodies against HAdV-3 are mainly directed against the hexon protein, which is not present in ADDomer made only of penton bases.

A potentially detrimental impact of pre-existing immunity on the immunogenicity of adenovirus-based viral vectors has been described,^{45,46} which thus led us to explore whether such effect may also be encountered with our adenovirus-derived VLP platform.

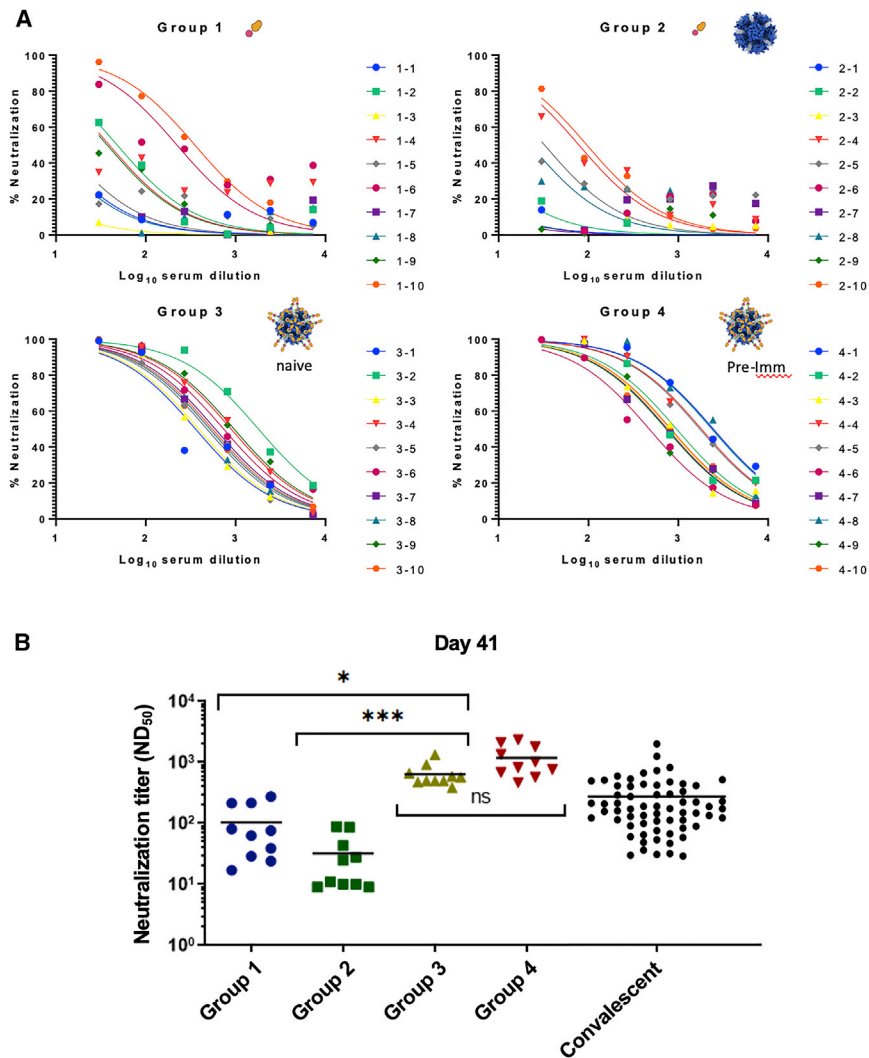


Figure 7. Neutralization study of mice sera on SARS-CoV-2 pseudo-typed virus and comparison with COVID-19 convalescent patients

(A) Curves showing the percentage of neutralization of individual sera of mice from all groups on viral infection by SARS-CoV-2 pseudo-typed virus. This pseudo-typed virus encodes luciferase as a reporter of cell infection and was preincubated with three-time serial dilutions of sera. Luciferase expression was compared to the one of non-neutralized virus. (B) Comparison of the neutralization titer at 50% of the maximal effect (ND₅₀) from all individual mice with the mean represented by a line. Statistical analysis using Kruskal-Wallis tests followed by a Dunn's multiple comparison tests demonstrates the superiority of neutralization of sera from mice immunized with RBD-decorated ADDomer particles versus both non-decorated particles and COVID-19 convalescent patients.

contrast to current platforms using the ST/SC system, we opted to engineer the ST on the VLP side, within the exposed VL. Thanks to this design, it can be envisaged to add another ST in a second exposed loop, such as the RGD (RGDL), to further increase stoichiometry (up to 120 attachment sites). Moreover, for mosaic vaccine approaches, the RGDL can be used to insert another orthogonal attachment site such as a snoop tag to display a second antigen. As an added value, the use of two different attachment tags/loops allows for differential antigenic stoichiometries and display patterns. Indeed, the RGDLs are more central on the pentameric building block of the ADDomer than the VLs, which are exposed on the periphery, resulting in a greater distance between the VLs than the RGDLs at the pentamer level.

Interestingly, in contrast to adenovirus-viral vectors, pre-immunity against the VLP had no detrimental effect on the immunogenicity of our adenovirus-inspired VLP platform. Indeed, mice with immunity to ADDomer at the time of the first immunization appeared to respond with somehow greater Ab titers against RBD than naive mice, although the difference was not found significant (group 4 versus group 3, Figure 5C). This potential beneficial effect may be in particular explained by the formation of immune complexes leading to a better uptake by antigen-presenting cells, via Fc receptors, resulting in an increase in immunogenicity.⁴⁷ Of note, the prevalence, in individuals who have been infected with HAdV-3, of antibodies directed against the penton base, which is the only component of ADDomer, is not precisely known. Our present work anticipates that our platform could be used whatever the HAdV-3 immunological status of the patients, and the potential presence of anti-penton antibodies.

In conclusion, we designed a new adenovirus-inspired VLP platform that achieves high immunogenicity against the displayed antigen. In

Displaying antigens through attachment to these two loops will therefore lead to various patterns of antigen display at the VLP scale, as shown in Figure S5. This will offer a large range of combinations to vary the stoichiometry of decoration as well as the distance between the antigens to potentially optimize immunogenicity.⁴⁸ The versatility of the vaccine platform can thus be exploited to generate mosaic particles displaying RBDs from different betacoronaviruses or SARS-CoV-2 variants to broaden NAb responses and protect against current and future variants of concern. A recent work described that 60-mer mosaic nanoparticles with four to eight distinct RBDs from betacoronaviruses can be generated. Remarkably, the codisplay of the SARS-CoV-2 RBD along with other RBDs showed that the combination of antigens on the same particle did not affect the elicitation of neutralizing antibodies against a particular RBD.³⁷ Moreover, neutralization of both "matched" and "mismatched" strains was observed after mosaic priming, suggesting that such particles might protect against several betacoronaviruses at once after a single injection.

More generally, our new versatile platform constitutes a putative tool in the preparedness to fight emerging pathogens that will remain to be investigated in viral challenge trials.

MATERIALS AND METHODS

Baculovirus production

The baculovirus expression system was used for both the production of ADDomer-SpyTag (ADD-ST) and for the RBD fused to SpyCatcher (RBD-SC). Synthetic DNA (Genscript) was cloned in the pACEBac1 using the restriction sites BamHI and HindIII. For RBD-SC, the SARS-CoV-2 spike sequence (320–554) was cloned upstream of the SC, and a hexa His-Tag was added in the C-terminus of SC. This fusion protein was secreted using the melittin signal peptide present in the vector. Recombinant baculoviruses were made by transposition with an in-house bacmid expressing yellow fluorescent protein, as previously described.⁵ Baculovirus was amplified on Sf21 cells at low multiplicity of infection (MOI) and after two amplification cycles was used to infect insect cells for 64 to 72 h at high MOI. For ADD-ST production, the infected cells were pelleted and recovered, whereas for RBD-SC, cells were discarded and the supernatant was saved.

Protein purification

ADDomer and ADD-ST purification

The ADDomer and ADD-ST were purified according to classical protocol.⁴⁹ Briefly, after lysis of the insect cell pellet by three cycles of freeze-thaw in the presence of Complete protease inhibitor cocktail (Roche), and removal of debris, the lysate was loaded onto a 20% to 40% sucrose density gradient. The gradient was centrifuged for 18 h at 4°C on an SW41 Rotor in a Beckman XPN-80 ultracentrifuge. The dense collected fractions at the bottom of the tubes were dialyzed against Hepes 10 mM pH 7.4, NaCl 150 mM, and then loaded onto a Macroprep Q cartridge (Bio-Rad). After elution by a 150- to 600-mM linear NaCl gradient in Hepes 10 mM pH 7.4, ADDomer-containing fractions were checked by SDS-PAGE and concentrated on Amicon (MWCO: 100 kDa) with buffer exchange to Hepes 10 mM pH 7.4, NaCl 150 mM.

SC purification

After lysis of the insect cell pellet as described above in the presence of Complete EDTA-free protease inhibitor cocktail, the clarified lysate was diluted five times in wash buffer (Hepes 10 mM pH 7.4, NaCl 150 mM, imidazole 10 mM) and loaded onto a His Gravitrapp column (Cytiva) by gravity, with two passages of the lysate onto the column. The column was washed with the same buffer, then eluted by 200 mM Imidazole. The fractions were analyzed by SDS-PAGE, pooled, and Imidazole was withdrawn by buffer exchange using Amicon ultrafiltration devices (MWCO: 4 kDa).

RBD-SC purification

The insect cell supernatant was centrifuged after thawing for 15 min at 7,500 g and loaded onto a Hepes 10 mM pH 7.4 pre-equilibrated Heparin column (Cytiva) of 5 mL for 500 mL of supernatant. The column was washed with Hepes 10 mM pH 7.4

for 25 mL then eluted for 10 mL with 0 to 500 mM linear NaCl gradient in Hepes 10 mM pH 7.4. The eluate was supplemented with 30 mM Imidazole-HCl and incubated with Ni-NTA beads (Qiagen), 2 mL of beads for 500 mL culture, for at least 1 h at 4°C under gentle agitation. The beads were then poured into an empty column and the protein was eluted by two column volumes of 250 mM Imidazole in Hepes 10 mM pH 7.4, NaCl 150 mM. It was then submitted to buffer exchange using an Amicon device (MWCO 30 kDa).

RBD purification

The following reagent was produced under HHSN272201400008C and obtained through BEI Resources, NIAID, NIH: Vector pCAGGS containing the SARS-CoV2, Wuhan-Hu-1 Spike Glycoprotein RBD, NR-52309. Vector NR-52309 from BEI Resources was used for mammalian expression of the RBD alone used for ELISA. EXPI293 cells grown in EXPI293 expression medium were transiently transfected with the vector according to the manufacturer's protocol (Thermo Fisher Scientific). Five days after transfection, the medium was recovered and filtered through a 0.45-µm filter. Two-step protein purification on Aktä Xpress, with a HisTrap HP column (GE Healthcare) and a Superdex 75 column (GE Healthcare) was performed using 20 mM Tris pH 7.5 and 150 mM NaCl buffer. For the HisTrap, a wash step in 75 mM imidazole was performed and RBD was eluted in buffer supplemented with 500 mM imidazole before loading onto the gel filtration column run in equilibration buffer.

N-glycosidase treatment

RBD-SC was incubated for 1 h at 37°C with the N-glycosidase PGNase F (kindly provided by Dr Nicole Thielens) at 1:100 ratio, then run on gel next to the same amount of untreated RBD-SC.

Complex formation

ADD-SpyTag + SpyCatcher (ADD-ST/SC) for Cryo-EM

The purified ADD-ST was mixed with an excess of purified SC (ratio 1:4). The protein mix was incubated overnight at 25°C under shaking in a Thermomixer (300 rpm). A purification step on a sucrose gradient was performed to remove the SC in excess and to recover only the fully decorated ADD-ST/SC at the bottom of the gradient. Buffer exchange was done in 10 mM Hepes, 150 mM NaCl, and the sample was concentrated to 1.5 mg/mL.

ADD-SpyTag + SpyCatcher-RBD (ADD-RBD) for

characterization and mice immunization experiments

Covalent complex formation was obtained by incubation of purified ADD-ST with purified RBD protein fused to SC (RBD-SC). Incubation was performed at 25°C under agitation on a Thermomixer at 300 rpm. RBD-SC ratio per ADD-ST was varied according to the experiment, as indicated in the text. For immunization experiments, a ratio of 40 copies of RBD-SC per ADD-ST was chosen to leave minimal free RBD-SC. This ratio was calculated on SDS-PAGE using ImageLab software (Bio-Rad). Integrity of the ADD-RBD was checked by negative staining electron microscopy.

In vivo experiments and vaccination

Vaccination experiments were performed according to ethical guidelines, under a protocol approved by the Grenoble Ethical Committee for Animal Experimentation and the French Ministry of Higher Education and Research (reference number: APAFIS#27765–2020102114206782 v2). Five-week-old female Balb/c mice were purchased from Janvier (Le Genestet St. Isle, France). For all mice groups, vaccines were in PBS and adjuvanted with one volume of ADDavax (InvivoGen). All the mice received two vaccine doses at 2 weeks of interval (day 0 and day 14) starting at 8 weeks of age. Each mice group received subcutaneously the corresponding vaccine as indicated within the paper in 100 μ L final volume, in the right flank. The pre-immunized group received 2 weeks before the first dose of vaccine (day –15) the ADDomer vector alone (5 μ g in 100 μ L final volume, in the right flank). The day before each vaccination, and 2 and 4 weeks after the last vaccination, 100 μ L of blood was withdrawn for serologic tests. For retro-orbital blood sampling, mice were anesthetized with 4% Isoflurane.

ELISA

The antigens (either RBD or ADDomer) were diluted at 1 μ g/mL in PBS, and 50 μ L was coated overnight at 4°C, in a 96-well plate (Maxisorp NUNC Immunoplate, #442404). Plates were washed using a ThermoScientific Microplate washer (#5165040). After three washes with 100 μ L of PBS-Tween 0.05%, plates were blocked with PBS-BSA 3% for 1 h. Mouse serum was serially diluted in PBS and incubated for 1 h (50 μ L/well) at room temperature. After five washes with PBS-Tween 0.05%; a goat anti-mouse IgG (H + L) secondary Ab linked to horseradish peroxidase (JIR 115-035-062) diluted at 1:2,500 in PBS-Tween 0.05% was added for 1 h. After five washes, 50 μ L of transmembrane domain substrate was distributed per well. The enzymatic reaction was stopped after 70 s by addition of 50 μ L of H₂SO₄ (1 M), and plates were read at 450 nm with a TECAN Spark 10M plate reader.

Electron microscopy

Negative staining

Samples of 3.5 μ L were adsorbed on the clean side of a carbon film previously evaporated on mica and then stained using 2% (w/v) Sodium Silico Tungstate pH 7.4 for 30 s. The sample/carbon ensemble was then transferred to a grid and air-dried. Images were acquired under low-dose conditions (<30 e[–]/Å²) on an F20 electron microscope operated at 120 kV using a CETA camera.

Cryo-EM

Quantifoil grids (300 mesh, R 1.2/1.3) were negatively glow-discharged at 30 mA for 45 s; 3.5 μ L of the sample were applied onto the grid, and excess solution was blotted away with a Vitrobot Mark IV (FEI) (blot time: 6 s, blot force: 0, 100% humidity, 20°C), before plunge-freezing in liquid ethane. The grid was transferred onto a 200-kV Thermo Fisher Glacios microscope equipped with a K2 summit direct electron detector for data collection. Automated data collection was performed with SerialEM, acquiring one image per hole, in counting mode. Micrographs were recorded at a nominal \times 36,000 magnification, giving

a pixel size of 1.145 Å (calibrated using a β -galactosidase sample) with a defocus ranging from –0.6 to –2.35 μ m. In total, 1,038 movies with 40 frames per movie were collected with a total exposure of 40 e[–]/Å².

Image processing and cryo-EM structure refinement

Movie drift correction was performed with Motioncor2⁵⁰ using frames from 2 to 40. CTF determination was performed with Relion 3.1.2 (Scheres 2012). A total of 939 movies of 1,038 were kept at this stage. Particle selection was done using the Laplacian filter with a diameter between 30 and 40 nm. A total of 77,323 particles were automatically selected, boxed into 480 \times 480-pixel² boxes and submitted to 2D classification. After extensive selection and generation of an initial model imposing I1 symmetry, 3D refinement followed by CTF Refine and post-processing generated a final reconstruction including 10,163 particles with a resolution of 2.76 Å (Fourier Shell = 0.143) (applied B-factor –82)

Immunofluorescence microscopy

HeLa-ACE2 cells (kindly provided by Dr David Nemazee) were seeded on polylysine-coated glass coverslips the day before the experiment. Coverslips were incubated for 1 h at 4°C with 0.75 μ g of either ADD-ST or ADD-RBD in 50 μ L of pre-chilled DMEM. Coverslips were washed three times in cold PBS then fixed for 10 min with –20°C methanol. Fixed cells were blocked for 1 h in PBS supplemented by 3% normal goat serum, then incubated for 1 h with 1:1,000 rabbit HAd3 anti penton base serum. After three PBS washes, cells were incubated with 1/250 antiRabbit Alexa 488 Ab (ThermoFisher A32721), washed three times in PBS, then nuclei were counterstained with Hoechst 33258 for 3 min before mounting. Observations were done on a Zoe microscope (Bio-Rad).

Surface plasmon resonance

Surface plasmon resonance experiment was performed on a T200 instrument. Anti-human Fc polyclonal antibody (Jackson ImmunoResearch, 109-005-008) diluted at 25 μ g/mL in 10 mM sodium acetate pH 5 was immobilized on CM5 sensor chips using the amine coupling chemistry according to the manufacturer's instructions (Cytiva) to get an immobilization level of 14,000 RU. ACE-2 –Fc (GenScript Z033484) was diluted at 1.2 μ g/mL in HBS P+ (Cytiva) to get an capture level of 100 RU. For interaction measurements, ADD-RBD (ranging from 1 nM to 11nM in HBSP+) was injected over captured ACE-2 Fc in HBS P+ buffer at 30 μ L/min. Anti-human Fc polyclonal antibody flow cell was used for correction of the binding response. Regeneration of the surfaces was achieved by 10 mM Glycine pH2. Binding curves were analyzed using BIAEvaluation software (GE Healthcare) and data was fit to a 1:1 Langmuir with drifting baseline interaction model.

Neutralization assays and pseudo-typed SARS-CoV-2 virion production

Pseudovirus production and titration

Neutralization assays were performed using lentiviral pseudotypes harboring the SARS-CoV-2 spike and encoding luciferase. Briefly,

gag/pol and luciferase plasmids were co-transfected with a SARS-CoV-2 spike plasmid with a C-term deletion of 18aa at 1:0.4:1 ratio on adherent HEK293T cells. Supernatants containing the produced pseudoviruses were harvested 72 h after transfection, centrifuged, filtered through 0.45 μm and concentrated 50 times on Amicon Ultra (MWCO 100KDa), aliquoted and stored at -80°C . Before use, supernatants were tittered using HeLa ACE-2 cells to determine the appropriate dilution of pseudovirus necessary to obtain about 150,000 relative light units (RLU) per well in a 48-well plate.

Neutralization assay

Serial 3-fold dilutions starting from 1/10 dilution (serum), or 6 $\mu\text{g}/\text{mL}$ (known bNAbs) were let in contact with the pseudoviruses for 1 h at 37°C in 96-w white plates (Greiner #675083), before addition of HeLa ACE2 cells. Plates were incubated 24 h at 37°C , protected from evaporation, then cells were fed with 60 μL of DMEM (Gibco 11,966-025) supplemented with 10% FBS (VWR 97068-086), and incubated for another 24 h. Medium in each well was aspirated and replaced by 45 μL of 1X cell lysis buffer (OZ Bioscience # LUC1000) for a 60-min incubation under agitation; 30 μL of luciferin substrate was then added and RLU was measured instantly by a luminometer. For competition with ADD-ST, ADD-RBD, and RBD-SC, the same protocol was used with initial concentration of 150 $\mu\text{g}/\text{mL}$ for ADD-ST, 200 $\mu\text{g}/\text{mL}$ and ADD-RBD and 50 $\mu\text{g}/\text{mL}$ for RBD-SC alone. Serums from a cohort of Grenoble region hospitalized convalescent patients were obtained with their consent, 6 to 8 months following COVID-19 diagnosis. The study was approved by the “Comité de Protection des Personnes SUD-EST I” on 20 August 2020 (ref 2020-84).

Statistical analyses

As the half maximal inhibitory concentration (IC₅₀) and median effective dose (ED₅₀) datasets followed a non-normal, heteroscedastic distribution, a non-parametric test was used for comparison of the different groups. Kruskal-Wallis tests were performed followed by a Dunn’s multiple comparison tests for each figure. Differences were considered significant when p value was below 0.05. Statistics were performed using GraphPad software, version 9.

SUPPLEMENTAL INFORMATION

Supplemental information can be found online at <https://doi.org/10.1016/j.ymthe.2022.02.011>.

ACKNOWLEDGMENTS

We are grateful to the “CNRS Prematuration program,” to the “ANR-Flash COVID” and to “Région Auvergne-Rhône-Alpes, AuRA” for the financial support to this work. This project has received funding from the European Research Council (ERC) under the European Union’s Horizon 2020 research and innovation program (grant agreement No 682286). D.H. is supported by GEFLUC Dauphiné-Savoie, Ligue contre le Cancer Comité Isère, Université Grenoble Alpes IDEX Initiatives de Recherche Stratégiques and Fondation du Souffle-Fonds de recherche en santé respiratoire (FdS-FRSR). We

thank Aymeric Peuch for help with the usage of the EM computing cluster and Emmanuelle Neumann for the training of C.C. in negative staining and Leandro Estrozi for help with image analysis. We thank Philippe Mas, Dr Matthieu Roustit, and Dr Sebastian Dergan-Dylon for help with statistical analysis. We thank David Nemazee for HeLa-ACE2 cells and SARS-CoV-2 spike expression plasmid, and Pierre Charneau for plasmids encoding for lentiviral proteins and luciferase. We thank Olivier Epaulard and Julien Lupo for the COVID-19 patients cohort study. This work used the platforms of the Grenoble Instruct-ERIC center (ISBG; UAR 3518 CNRS-CEA-UGA-EMBL) within the Grenoble Partnership for Structural Biology (PSB), supported by FRISBI (ANR-10-INBS-05-02) and GRAL, financed within the University Grenoble Alpes graduate school (Écoles Universitaires de Recherche) CBH-EUR-GS (ANR-17-EURE-0003). The electron microscope facility is supported by the Auvergne-Rhône-Alpes Region, the Fondation Recherche Medicale (FRM), the fonds FEDER and the GIS-Infrastructures en Biologie Sante et Agronomie (IBISA). I.B.S. acknowledges integration into the Interdisciplinary Research Institute of Grenoble (IRIG, CEA). V.D. has an internship of Master de Biologie, École Normale Supérieure de Lyon, Université Claude Bernard Lyon I, Université de Lyon, 69342 Lyon Cedex 07, France.

AUTHOR CONTRIBUTIONS

P.F., M.C.D., and P.P. conceived the experiments. Vector production and purification were performed by C.C., V.D., and S.G. Structural analysis was performed by G.S., D.F., and C.C. Animal experiments were performed by D.H. and S.B. Molecular interaction studies was performed by E.G., C.M., and E.V.S. Immunological characterization and virus neutralization was performed by A.A., I.B., and M.B. With input from all authors, P.F. and P.P. wrote the manuscript.

DECLARATION OF INTERESTS

We declare no competing interests.

REFERENCES

- Bok, K., Sitar, S., Graham, B.S., and Mascola, J.R. (2021). Accelerated COVID-19 vaccine development: milestones, lessons, and prospects. *Immunity* 54, 1636–1651.
- Nguyen, B., and Tolia, N.H. (2021). Protein-based antigen presentation platforms for nanoparticle vaccines. *NPJ Vaccin.* 6, 70.
- Fender, P., Ruigrok, R.W., Gout, E., Buffet, S., and Chroboczek, J. (1997). Adenovirus dodecahedron, a new vector for human gene transfer. *Nat. Biotechnol.* 15, 52–56.
- Besson, S., Vragneau, C., Vassal-Stermann, E., Dagher, M.C., and Fender, P. (2020). The adenovirus dodecahedron: beyond the platonic story. *Viruses* 12, 718.
- Vragneau, C., Bufton, J.C., Garzoni, F., Stermann, E., Rabi, F., Terrat, C., Guidetti, M., Josserand, V., Williams, M., Woods, C.J., et al. (2019). Synthetic self-assembling ADDomer platform for highly efficient vaccination by genetically encoded multi-epitope display. *Sci. Adv.* 5, eaaw2853.
- Zakeri, B., Fierer, J.O., Celik, E., Chittock, E.C., Schwarz-Linek, U., Moy, V.T., and Howarth, M. (2012). Peptide tag forming a rapid covalent bond to a protein, through engineering a bacterial adhesin. *Proc. Natl. Acad. Sci.* 109, E690–E697.
- Brune, K.D., Leneghan, D.B., Brian, I.J., Ishizuka, A.S., Bachmann, M.F., Draper, S.J., Biswas, S., and Howarth, M. (2016). Plug-and-Display: decoration of Virus-Like Particles via isopeptide bonds for modular immunization. *Sci. Rep.* 6, 19234.
- Li, L., Fierer, J.O., Rapoport, T.A., and Howarth, M. (2014). Structural analysis and optimization of the covalent association between SpyCatcher and a peptide tag. *J. Mol. Biol.* 426, 309–317.

9. Keeble, A.H., and Howarth, M. (2020). Power to the protein: enhancing and combining activities using the Spy toolbox. *Chem. Sci.* *11*, 7281–7291.
10. Zhou, P., Yang, X.-L., Wang, X.-G., Hu, B., Zhang, L., Zhang, W., Si, H.-R., Zhu, Y., Li, B., Huang, C.-L., et al. (2020). A pneumonia outbreak associated with a new coronavirus of probable bat origin. *Nature* *579*, 270–273.
11. Khoury, D.S., Cromer, D., Reynaldi, A., Schlub, T.E., Wheatley, A.K., Juno, J.A., Subbarao, K., Kent, S.J., Triccas, J.A., and Davenport, M.P. (2021). Neutralizing antibody levels are highly predictive of immune protection from symptomatic SARS-CoV-2 infection. *Nat. Med.* *27*, 1205–1211.
12. McMahan, K., Yu, J., Mercado, N.B., Loos, C., Tostanoski, L.H., Chandrashekar, A., Liu, J., Peter, L., Atyeo, C., Zhu, A., et al. (2021). Correlates of protection against SARS-CoV-2 in rhesus macaques. *Nature* *590*, 630–634.
13. Polack, F.P., Thomas, S.J., Kitchin, N., Absalon, J., Gurtman, A., Lockhart, S., Perez, J.L., Pérez Marc, G., Moreira, E.D., Zerbini, C., et al. (2020). Safety and efficacy of the BNT162b2 mRNA covid-19 vaccine. *N. Engl. J. Med.* *383*, 2603–2615.
14. Jackson, L.A., Anderson, E.J., Roupael, N.G., Roberts, P.C., Makhene, M., Coler, R.N., McCullough, M.P., Chappell, J.D., Denison, M.R., Stevens, L.J., et al. (2020). An mRNA vaccine against SARS-CoV-2 — preliminary report. *N. Engl. J. Med.* *383*, 1920–1931.
15. Heath, P.T., Galiza, E.P., Baxter, D.N., Boffito, M., Browne, D., Burns, F., Chadwick, D.R., Clark, R., Cosgrove, C., Galloway, J., et al. (2021). Safety and efficacy of NVX-CoV2373 covid-19 vaccine. *N. Engl. J. Med.* *385*, 1172–1183.
16. Shang, J., Ye, G., Shi, K., Wan, Y., Luo, C., Aihara, H., Geng, Q., Auerbach, A., and Li, F. (2020). Structural basis of receptor recognition by SARS-CoV-2. *Nature* *581*, 221–224.
17. Yan, R., Zhang, Y., Li, Y., Xia, L., Guo, Y., and Zhou, Q. (2020). Structural basis for the recognition of SARS-CoV-2 by full-length human ACE2. *Science* *367*, 1444–1448.
18. Lan, J., Ge, J., Yu, J., Shan, S., Zhou, H., Fan, S., Zhang, Q., Shi, X., Wang, Q., Zhang, L., et al. (2020). Structure of the SARS-CoV-2 spike receptor-binding domain bound to the ACE2 receptor. *Nature* *581*, 215–220.
19. Starr, T.N., Greaney, A.J., Hilton, S.K., Ellis, D., Crawford, K.H.D., Dingens, A.S., Navarro, M.J., Bowen, J.E., Tortorici, M.A., Walls, A.C., et al. (2020). Deep mutational scanning of SARS-CoV-2 receptor binding domain reveals constraints on folding and ACE2 binding. *Cell* *182*, 1295–1310.e20.
20. Piccoli, L., Park, Y.-J., Tortorici, M.A., Czudnochowski, N., Walls, A.C., Beltramelio, M., Silacci-Fregni, C., Pinto, D., Rosen, L.E., Bowen, J.E., et al. (2020). Mapping neutralizing and immunodominant sites on the SARS-CoV-2 spike receptor-binding domain by structure-guided high-resolution serology. *Cell* *183*, 1024–1042.e21.
21. Barnes, C.O., West, A.P., Huey-Tubman, K.E., Hoffmann, M.A.G., Sharaf, N.G., Hoffman, P.R., Koranda, N., Gristick, H.B., Gaebler, C., Muecksch, F., et al. (2020). Structures of human antibodies bound to SARS-CoV-2 spike reveal common epitopes and recurrent features of antibodies. *Cell* *182*, 828–842.e16.
22. Robbiani, D.F., Gaebler, C., Muecksch, F., Lorenzi, J.C.C., Wang, Z., Cho, A., Agudelo, M., Barnes, C.O., Gazumyan, A., Finkin, S., et al. (2020). Convergent antibody responses to SARS-CoV-2 in convalescent individuals. *Nature* *584*, 437–442.
23. Brouwer, P.J.M., Caniels, T.G., van der Straten, K., Snitselaar, J.L., Aldon, Y., Bangaru, S., Torres, J.L., Okba, N.M.A., Claireaux, M., Kerster, G., et al. (2020). Potent neutralizing antibodies from COVID-19 patients define multiple targets of vulnerability. *Science* *369*, 643–650.
24. Barnes, C.O., Jette, C.A., Abernathy, M.E., Dam, K.-M.A., Esswein, S.R., Gristick, H.B., Malyutin, A.G., Sharaf, N.G., Huey-Tubman, K.E., Lee, Y.E., et al. (2020). SARS-CoV-2 neutralizing antibody structures inform therapeutic strategies. *Nature* *588*, 682–687.
25. Alsoussi, W.B., Turner, J.S., Case, J.B., Zhao, H., Schmitz, A.J., Zhou, J.Q., Chen, R.E., Lei, T., Rizk, A.A., McIntire, K.M., et al. (2020). A potentially neutralizing antibody protects mice against SARS-CoV-2 infection. *J. Immunol.* *205*, 915–922.
26. Zost, S.J., Gilchuk, P., Case, J.B., Binshtein, E., Chen, R.E., Nkolola, J.P., Schäfer, A., Reidy, J.X., Trivette, A., Nargi, R.S., et al. (2020). Potently neutralizing and protective human antibodies against SARS-CoV-2. *Nature* *584*, 443–449.
27. O'Brien, M.P., Forleo-Neto, E., Musser, B.J., Isa, F., Chan, K.-C., Sarkar, N., Bar, K.J., Barnabas, R.V., Barouch, D.H., Cohen, M.S., et al. (2021). Subcutaneous REGEN-COV antibody combination to prevent covid-19. *N. Engl. J. Med.* *385*, e70.
28. Fuschiotti, P., Schoehn, G., Fender, P., Fabry, C.M.S., Hewat, E.A., Chroboczek, J., Ruigrok, R.W.H., and Conway, J.F. (2006). Structure of the dodecahedral penton particle from human adenovirus type 3. *J. Mol. Biol.* *356*, 510–520.
29. Lei, C., Qian, K., Li, T., Zhang, S., Fu, W., Ding, M., and Hu, S. (2020). Neutralization of SARS-CoV-2 spike pseudotyped virus by recombinant ACE2-Ig. *Nat. Commun.* *11*, 2070.
30. Epaulard, O., Buisson, M., Nemoz, B., Maréchal, M.L., Terzi, N., Payen, J.-F., Froidure, M., Blanc, M., Mounayar, A.-L., Quénard, F., et al. (2021). Persistence at one year of neutralizing antibodies after SARS-CoV-2 infection: influence of initial severity and steroid use. *J. Infect.* <https://doi.org/10.1016/j.jinf.2021.10.009>.
31. Tan, T.K., Rijal, P., Rahikainen, R., Keeble, A.H., Schimanski, L., Hussain, S., Harvey, R., Hayes, J.W.P., Edwards, J.C., McLean, R.K., et al. (2021). A COVID-19 vaccine candidate using SpyCatcher multimerization of the SARS-CoV-2 spike protein receptor-binding domain induces potent neutralising antibody responses. *Nat. Commun.* *12*, 542.
32. Kanekiyo, M., Wei, C.-J., Yassine, H.M., McTamney, P.M., Boyington, J.C., Whittle, J.R.R., Rao, S.S., Kong, W.-P., Wang, L., and Nabel, G.J. (2013). Self-assembling influenza nanoparticle vaccines elicit broadly neutralizing H1N1 antibodies. *Nature* *499*, 102–106.
33. Kanekiyo, M., Bu, W., Joyce, M.G., Meng, G., Whittle, J.R.R., Baxa, U., Yamamoto, T., Narpala, S., Todd, J.-P., Rao, S.S., et al. (2015). Rational design of an Epstein-Barr virus vaccine targeting the receptor-binding site. *Cell* *162*, 1090–1100.
34. Bachmann, M.F., and Zinkernagel, R.M. (1997). Neutralizing antiviral B cell responses. *Annu. Rev. Immunol.* *15*, 235–270.
35. Watanabe, Y., Allen, J.D., Wrapp, D., McLellan, J.S., and Crispin, M. (2020). Site-specific glycan analysis of the SARS-CoV-2 spike. *Science* *369*, 330–333.
36. Shinde, V., Bhikha, S., Hoosain, Z., Archary, M., Bhorat, Q., Fairlie, L., Lalloo, U., Masilela, M.S.L., Moodley, D., Hanley, S., et al. (2021). Efficacy of NVX-CoV2373 covid-19 vaccine against the B.1.351 variant. *N. Engl. J. Med.* *385*, 1172–1183.
37. Cohen, A.A., Gnanapragasam, P.N.P., Lee, Y.E., Hoffman, P.R., Ou, S., Kakutani, L.M., Keeffe, J.R., Wu, H.-J., Howarth, M., West, A.P., et al. (2021). Mosaic nanoparticles elicit cross-reactive immune responses to zoonotic coronaviruses in mice. *Science* *371*, 735–741.
38. Walls, A.C., Fiala, B., Schäfer, A., Wrenn, S., Pham, M.N., Murphy, M., Tse, L.V., Shehata, L., O'Connor, M.A., Chen, C., et al. (2020). Elicitation of potent neutralizing antibody responses by designed protein nanoparticle vaccines for SARS-CoV-2. *Cell* *183*, 1367–1382.e17.
39. He, L., Lin, X., Wang, Y., Abraham, C., Sou, C., Ngo, T., Zhang, Y., Wilson, I.A., and Zhu, J. (2021). Single-component, self-assembling, protein nanoparticles presenting the receptor binding domain and stabilized spike as SARS-CoV-2 vaccine candidates. *Sci. Adv.* *7*, eabf1591.
40. Salzer, R., Clark, J.J., Vaysburd, M., Chang, V.T., Albecka, A., Kiss, L., Sharma, P., Gonzalez Llamazares, A., Kipar, A., Hiscoc, J.A., et al. (2021). Single-dose immunisation with a multimerised SARS-CoV-2 receptor binding domain (RBD) induces an enhanced and protective response in mice. *FEBS Lett.* *595*, 2323–2340.
41. Saunders, K.O., Lee, E., Parks, R., Martinez, D.R., Li, D., Chen, H., Edwards, R.J., Gobeil, S., Barr, M., Mansouri, K., et al. (2021). Neutralizing antibody vaccine for pandemic and pre-emergent coronaviruses. *Nature* *594*, 553–559.
42. Vogels, R., Zuijgeest, D., van Rijnsoever, R., Hartkoorn, E., Damen, I., de Béthune, M.-P., Kostense, S., Penders, G., Helmus, N., Koudstaal, W., et al. (2003). Replication-deficient human adenovirus type 35 vectors for gene transfer and vaccination: efficient human cell infection and bypass of preexisting adenovirus immunity. *JVI* *77*, 8263–8271.
43. Arnberg, N. (2012). Adenovirus receptors: implications for targeting of viral vectors. *Trends Pharmacol. Sci.* *33*, 442–448.
44. Haque, E., Banik, U., Monwar, T., Anthony, L., and Adhikary, A.K. (2018). Worldwide increased prevalence of human adenovirus type 3 (HAdV-3) respiratory infections is well correlated with heterogeneous hypervariable regions (HVRs) of hexon. *PLoS ONE* *13*, e0194516.
45. Lanzi, A., Ben Youssef, G., Perricaudet, M., and Benihoud, K. (2011). Anti-adenovirus humoral responses influence on the efficacy of vaccines based on epitope display on adenovirus capsid. *Vaccine* *29*, 1463–1471.

46. Anchim, A., Raddi, N., Zig, L., Perrieau, P., Le Goffic, R., Ryffel, B., and Benihoud, K. (2018). Humoral responses elicited by adenovirus displaying epitopes are induced independently of the infection process and shaped by the toll-like receptor/MyD88 pathway. *Front Immunol.* *9*, 124.
47. Heyman, B. (2003). Feedback regulation by IgG antibodies. *Immunol. Lett.* *88*, 157–161.
48. Veneziano, R., Moyer, T.J., Stone, M.B., Wamhoff, E.-C., Read, B.J., Mukherjee, S., Shepherd, T.R., Das, J., Schief, W.R., Irvine, D.J., et al. (2020). Role of nanoscale antigen organization on B-cell activation probed using DNA origami. *Nat. Nanotechnol.* *15*, 716–723.
49. Fender, P. (2014). Use of dodecahedron “VLPs” as an alternative to the whole adenovirus. *Methods Mol. Biol.* *1089*, 61–70.
50. Zheng, S.Q., Palovcak, E., Armache, J.-P., Verba, K.A., Cheng, Y., and Agard, D.A. (2017). MotionCor2: anisotropic correction of beam-induced motion for improved cryo-electron microscopy. *Nat. Methods* *14*, 331–332.